Understanding spatio-temporal barrier dynamics through the use of multiple shoreline proxies

[1]Pollard J.A., [1]Spencer, T., [2]Brooks, S.M., [1]Christie, E.K., and [3]Möller, I.

[1.] Department of Geography, University of Cambridge, Downing Place, Cambridge CB2 3EN, UK. jp646@cam.ac.uk, ts111@cam.ac.uk, ekc28@cam.ac.uk
[2.] Department of Geography, Birkbeck, University of London, Malet Street, London WC1E 7HX, UK. s.brooks@bbk.ac.uk
[3.] Department of Geography, Museum Building, Trinity College Dublin, Dublin 2, Ireland. moelleri@tcd.ie

Corresponding author: James A Pollard (jp646@cam.ac.uk)

Highlights

- **Five shoreline proxies are extracted for the Blakeney Point gravel barrier, east coast, UK.**
- **Multi-proxy analysis leads to enhanced understanding of coastal dynamics.**
- **Over centennial timescales, Blakeney Point shifts from drift to swash-alignment.**
- **Extensive washover deposits indicate periodic storm-driven retreat.**
- **Single-proxy analysis may result in a narrow understanding of coastal dynamics.**

Abstract

At the coast, risk arises where, and when, static human developments are situated within dynamic surroundings. Barrier islands are often sites of heightened coastal risk since they frequently support substantial human populations and undergo extensive morphological change owing to their low-lying form and persistence in energetic hydrodynamic and meteorological conditions. Using the mixed sand-gravel barrier of Blakeney Point, this study argues that to avoid an only partial understanding of coastal zone processes, it is necessary to make use of multiple shoreline proxies, capturing processes operating both at different timescales and different cross-shore positions. Here, five shoreline proxies were extracted from three data sources. Shoreline error was quantified and compared to observed shoreline change rates to establish proxy-specific, appropriate timescales for shoreline change analysis. The map derived Mean High Water Line at Blakeney Point revealed landward retreat of -0.61 m a^{-1} over the past 130 years with a shift from drift- towards swash-alignment of the barrier since 1981. Over the past 24 years, the High Water Line, Ridge Line and Vegetation Line reveal proxy-specific response to management regime change. The termination of barrier reprofiling of the eastern section of the barrier has resulted in increased sediment release to the downdrift barrier terminus, buffering retreat there at the expense of the updrift section. The Vegetation Line represents an effective proxy for storm-driven overwash with maximum shoreline retreat during surge events of 172 m, illustrating a strong event-driven component to barrier morphodynamics. By comparison to the other proxies, the LiDAR (Light Detection and Ranging) derived Mean High Water Line offers relatively limited insights into barrier dynamics, emphasising the importance of multi-proxy approaches. In the face of technological advance, we demonstrate the continued importance of critical attention towards the dependencies that exist between shoreline proxy selection and the processes that can be observed as a result.

Keywords (max. 6)

Barrier island; shoreline proxy; shoreline change; shoreline error

1. Introduction

Barrier islands are characteristic of 10% of continental shorelines, existing most frequently on coastal plains and in wave-dominated settings (Stutz and Pilkey, 2011). Many barrier islands

are densely populated, providing the foundations for expanding human populations (Neumann et al., 2015), delivering protection to landward shorelines (Grzegorzewski et al., 2011), and supporting ecologically valuable saline, brackish, and freshwater wetland habitats (Orford and Jennings, 1998). In a geomorphological sense, barrier systems reflect a complex interplay between contemporary barrier morphodynamics (longshore extension, landward rollover, response to management regime change), geological constraints (seen through variable erodability, sediment supply, and shoreface morphology) and human interventions.

Understanding spatio-temporal barrier dynamics requires the assessment of the relative importance of chronic (i.e. long-term, evolutionary trajectories) and acute (i.e. impact of extreme events) landform change and their interaction. Observation and monitoring campaigns must, therefore, measure a diversity of system variables, covering appropriate timescales, at sufficient spatial resolution. Capturing coastal dynamics through shoreline mapping is one of the enduring analytical approaches to this problem (Harley, 1975; Oliver, 1996). While numerous coastal proxies can be measured (e.g. Carapuço et al., 2016), a persistent focus on shorelines derives from i) the transferability of techniques across varied coastal environments (e.g. sandy shores (Hapke et al., 2016); soft rock cliffs (Brooks and Spencer, 2010); gravelly tidal inlets (Burningham, 2015); mangrove forest margins (Fromard et al., 2004); salt marsh – mudflat transitions (Van der Wal et al., 2008); and atoll island margins (Duvat and Pillet, 2017)) and ii) an ability to extract shorelines from varied data sources even where monitoring frequency is intermittent. Although this approach only directly captures dynamics in a certain portion of the coastal tract (Cowell et al., 2003), shoreline change has been demonstrated as a reliable proxy for volumetric change in a variety of sandy beach settings (Durán et al., 2016; Farris and List, 2007).

Recent technological advances, particularly through various forms of remote sensing, has increased the variety of data sources from which shorelines can be mapped (Dolan et al., 1980; Pollard et al., 2018; Stockdon et al., 2002). Routine shoreline extraction from vertical aerial photography has been ongoing since the post-WWII era, though earlier comments on the potential of aerial photography for understanding coastal systems pre-date this time (e.g. Oliver, 1924). More recently, the manipulation of digital elevation models (DEMs) from Light Detection And Ranging (LiDAR) datasets has proven valuable for quantifying not only shoreline but also beach volumetric change (Stockdon et al., 2002). At a local scale, unmanned autonomous vehicles provide capabilities for rapid, and potentially event-response level, shoreline mapping (Casella et al., 2016). At the global scale, improved computing power and data analysis platforms such as Google Earth Engine (Gorelick et al., 2017) are facilitating analysis of satellite datasets that stretch back to the 1970s with capture frequencies at monthly to weekly intervals (Luijendijk et al., 2018; Mentaschi et al., 2018; Vos et al., 2019).

Before conducting shoreline change analysis, it is necessary to define and extract shorelines from the data sources described above. Such decisions reflect data source availability, the

coastal environment in question, and the intended outcomes of the research. Consequently, shoreline proxies are specific to the research context in which decisions over their definition and extraction are made. Regarding shoreline definition, it is possible to identify two classes, proxy-based and datum-based shorelines. Proxy-based shorelines are visually discernible signatures whereas datum-based shorelines represent the intersection of a given tidal level with a specified vertical elevation (Boak and Turner, 2005). Proxy-based shorelines include shore features such as drift-lines (used to obtain the HWL), vegetation lines, cliff lines and ridge lines; while datum-based shorelines require the computation of a particular tidal elevation such as the mean high water line (MHWL) or mean high water springs (MHWS). Several studies have sought to establish the differences in shoreline position that arise from the extraction of the proxy-based shorelines in comparison to datum-based alternatives (e.g. Moore et al., 2006; Pajak and Leatherman, 2002; Robertson et al., 2004). These studies have established that shoreline proxies record coastal processes selectively, resulting in proxy-dependent offsets in shoreline position. Thus, for example, the drift line will record variations in tidal range, wave run-up and beach slope which occur daily and with high alongshore variability (Parker, 2003), while a time-averaged MHWL datum will filter out these shorter term effects. Positional offsets between different shorelines have been found to range from less than 1 m (Robertson et al., 2004) to over 50 m (Morton et al., 2004), with the largest offsets occurring on gentle sloping beaches, characterised by large waves and associated run-up (Moore et al., 2006; Morton et al., 2004).

The location-specific and instantaneous nature of these interferences presents a challenge for recent satellite-derived shoreline studies (Luijendijk et al., 2018; Vos et al., 2019). Cloud cover, waves, and sediment properties (moisture content, grain size) have been identified as key environmental drivers of inaccuracy when extracting satellite-derived shorelines (Hagenaars et al., 2018). Luijendijk et al. (2018) note that in locations with persistent swell or wave generated foam, satellite-derived shorelines tend to be located seawards of their actual position (although the impact of this offset is limited where this effect is persistent or when shoreline change is calculated over extended periods). Also working at the global scale, Vos et al. (2019) explicitly address the impact of tidal stage on satellite-derived shoreline position using a tidal correction term which standardises for tidal position between individual satellite images. Variability in shoreline position is also captured by looking at the signal to noise ratio between the typical magnitude of shoreline change at a given site and timescale (from one month to one decade) and the measurement error (which is calculated at approximately 10 m globally).

The examples above illustrate that the selection of particular shoreline proxies will determine which coastal processes are observed. Coastal setting exerts a first order control on the shoreline proxies that can be extracted since different processes characterise different coastal environments. For example, a barrier island setting may exhibit certain characteristic features that are amenable to measurement such as a dune line, barrier ridge, and back

barrier vegetated zone (Otvos, 2012). By measuring changes to these descriptors, it is possible to capture processes, such as overwash and landward rollover, that are themselves specific to barrier island settings (Masselink and Van Heteren, 2014; Schwartz, 1975). Within a given coastal setting, different proxies tend to represent different cross-shore locations along a continuum – the 'coastal tract' (Cowell et al., 2003) - of marine-to-terrestrial process controls. Often proxies encode transitions between different cross-shore zones, with changes in their position being determined by a different mix of drivers whose dominance varies cross-shore. Consequently, selecting a single shoreline to represent the complexity of coastal zone processes is inadvisable. Although various shoreline proxies have often been contrasted in the shoreline change literature (for example, Moore et al. (2006); Robertson et al. (2004); and Ruggiero et al. (2003) compared the HWL to a LiDAR derived MHWL), relatively little attention has been directed towards the different coastal processes that may be captured by different shoreline proxies. To explore the dependencies between the selection of particular shoreline proxies, and the coastal processes which are captured as a result, in this contribution we address three objectives:

i. Define a selection of proxy- and datum-based shorelines spanning annual to centennial timescales
ii. Quantify the error associated with each of the shoreline proxies
iii. Undertake shoreline change analysis to characterise the geomorphological processes captured by each of the shoreline proxies

The value of linking shoreline proxies and coastal processes is illustrated through reference to Blakeney Point, a mixed sand-gravel barrier on the coastline of eastern England, UK. Blakeney Point was chosen firstly, owing to its emplacement under decelerating Holocene sea level rise, an evolutionary pathway which is shared with many barriers globally (Carter et al., 1987; Hoyt, 1967). Furthermore, the contemporary sedimentary (e.g. sediment size and supply) and process environment (e.g. occurrence of storm events) of Blakeney Point has given rise to characteristic landscape features (e.g. barrier beach, vegetated dunes, back barrier wetlands) which permit comparison with barrier islands elsewhere (Otvos, 2012). Finally, recent management regime changes at Blakeney Point facilitate insight to both interventionist coastal management (as seen elsewhere in the UK (Hudson and Baily, 2018; Scott et al., 2016) and globally (Bergillos et al., 2017)) and the 'building with nature' approach which seeks to increase the role of natural processes to deliver sustainable coastal environments (Burgess and Kilkie, 2015; Cheong et al., 2013; de Vriend et al., 2014). Each of these characteristic features is elaborated below.

1.1 Regional setting

The barrier coastline of North Norfolk stretches for 45 km between the Chalk outcrop at Old Hunstanton and Kelling Hard (Figure 1A, B). During the Holocene, offshore of the North Norfolk coast, sea level rose from ca. -41 m at 10.75 ka BP to ca. -23 m at 8.3 ka BP, a mean

rate of 7.3 mm a^{-1} (Shennan et al., 2000, 2018). A slowing of sea level rise around 7 ka BP (Shennan et al., 2000), combined with a plentiful supply of sediments of glacial origin (Moorlock et al., 2008), set in train the development of a 2 km wide Holocene sedimentary prism including the prominent coastal features of Scolt Head Island and Blakeney Point (Allison, 1989). Similar Holocene evolutionary pathways have been proposed for barrier systems off the coast of Nova Scotia (Carter et al., 1990), western Ireland (Carter et al., 1989), southern England (Jennings et al., 1998), and southern Argentina (Isla and Bujalesky, 2000).

Blakeney Point is a 13 km long shingle spit, which stretches from the shore at Kelling Hard out into the sea at a high angle to the mainland, terminating offshore between the landward villages of Morston and Stiffkey (Oliver, 1913). The back-barrier area is characterized by relict spit recurves, with intervening back-barrier salt marsh, that extend landwards at high angles to the main beach. Recent westward extension of the spit has been characterized by beach and aeolian sand deposition, giving the terminus of the barrier a rather different character to the mixed gravel sandy ridge that dominates much of the spit's length to the east (Hardy, 1964). This terminal complex of ridges and dunes was deliberately excluded from the shoreline change analysis because of difficulties in defining and extracting shorelines here due to the highly mobile sand and shingle that comprises this part of the spit (Figure 1C).

The North Norfolk coast experiences a macro-tidal regime (MSTR = 4.7 m at Cromer, 20 km to the east) and a moderate wave climate. During the period November 2006 to November 2009, when a nearshore wave buoy was installed at Cley (7 m water depth), mean significant wave height varied from 0.55 – 0.72 m, with the largest waves driven by northerly winds and associated long fetch (Environment Agency, 2014). However, the coast is also vulnerable to relatively infrequent extreme water level events in the form of storm surges; in the period 1883-2014, twenty-one surge events had substantial societal impacts (Brooks et al., 2016). These surges may be accompanied by increased wave activity. Offshore mean significant wave heights at Blakeney Overfalls Wave rider buoy (25 m water depth, 10.5 km offshore) are typically 0.8 – 1.0 m (November 2006 to November 2009 (Environment Agency, 2014)) but peak wave heights of up to 3.8 m, 3.5 m, and 3.9 m were recorded during the 5 December 2013, 8 November 2007, and 17 March 2007 storm events respectively (Brooks et al., 2016). Numerical modelling suggests even higher significant wave heights during the surge of 31 January-1 February 1953, reaching up to 7.8 m offshore of the Norfolk coast (Wolf and Flather, 2005).

Observations of barrier systems elsewhere have established an important role for infrequent, high magnitude storm events in determining barrier evolution (Masselink and Van Heteren, 2014; Orford and Jennings, 1998; Orford et al., 1995). This derives from the sediment transport potential of energetic hydrodynamic events which can introduce qualitatively different barrier behaviours such as overwashing or breaching (Muir Wood and Bateman, 2005; Phillips and Van Dyke, 2016; Phillips, 2014; Schwartz, 1975). At Blakeney Point, some of

the first accounts of the morphological impacts of storm events relate to the winter of 1911-12. Oliver (1913) notes that the western terminus of the spit was reformed into a hook, reminiscent of the collection of recurves known as 'the Hood'. Further east, the same storm resulted in rollover of the gravel barrier and resultant landward retreat (Hill and Hanley, 1914). The Cley-Salthouse barrier is also vulnerable to breaching, documented as having taken place in 1897, 1953, 1978 and 2013 (Spencer et al., 2015). In addition to more conventional storms that approach from the north-westerly direction, easterly winds such as those experienced in 2018 during the late February to early March 'Beast from the East' have been observed to effect extensive coastal change, even in the absence of elevated water levels (Brooks and Spencer, 2019). For example, persistent easterly winds facilitated natural closure of two breaches within two months along the Cley-Salthouse barrier following the storm surge of 5 December 2013 (Spencer et al., 2015).

Coastal barriers have been identified as effective forms of coastal risk reduction owing to their morphosedimentary characteristics (Buscombe and Masselink, 2006), including erosion-resistance, coarse grained composition, and associated high percolation rates which give rise to naturally steep, energy reflective forms (Powell, 1990; Van Wellen et al., 2000). Consequently, many gravel barriers have been actively managed to enhance and maintain their protective functions (Ahrens, 1990; Aminti et al., 2003; Mason and Coates, 2001; Masselink et al., 2014) In terms of management regime (Figure 1C), Blakeney Point can be broadly divided into two sections. To the east of Cley, the Cley-Salthouse barrier was actively reprofiled from the 1950s to maintain the crest height at ca. 8-9 m ODN (Ordnance Datum Newlyn where 0.0 m ODN approximates to sea level; Bradbury and Orford, 2007). However, reprofiling was terminated after the winter of 2005 to encourage a resumption of natural processes (Environment Agency, 2010). The shift towards a less interventionist management regime aligns with the local and national strategy seeking to increase the proportion of coastal realignment sites in preference to hard engineered alternatives (Defra, 2006; Hudson and Baily, 2018). To the west of Cley, the barrier has remained unmanaged at all times and is typified by a crest height of ca. 5-6 m ODN (Bradbury and Orford, 2007). The two sections also differ in terms of hydrodynamic forcing on the landward side of the barrier. The western section is exposed to tidal flows from the Blakeney Channel while the eastern section is not, being backed by coastal and freshwater grazing marshes.

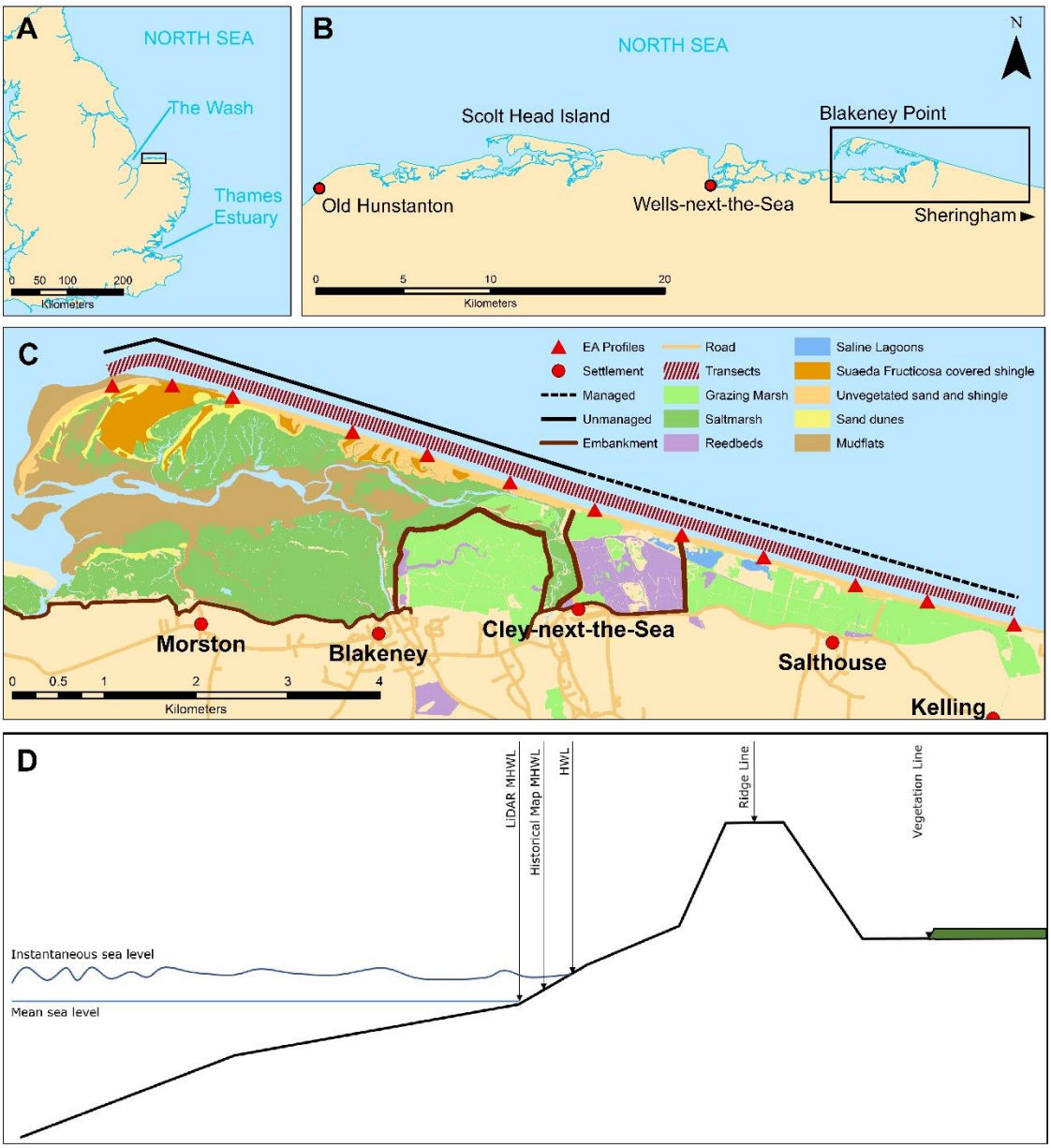

Figure 1: Regional setting map. A: The UK east coast; B: the North Norfolk coast with larger settlements marked; C: Blakeney Point annotated with shoreline change analysis transects, indicative management regime zones, selected UK Environment Agency cross-shore topography profiles, habitat types, coastal defence structures, roads and settlements. D: simplified cross-shore profile marked with indicative shoreline proxies.

2. Methodology

2.1 Shoreline definition

Five distinct shoreline definitions were devised (Figure 1D). The definitions reflect the data sources from which the shorelines are extracted and to some extent the coastal environment of Blakeney Point. The shoreline proxy present on historical maps is the Mean High Water Line (MHWL) as mapped by Ordnance Survey surveyors (see Oliver (1996) and Sutherland (2012) for surveying procedures). Three different shoreline proxies were extracted from the vertical aerial photographs: the High Water Line (HWL), defined as the wet/dry line created

by high tide prior to aerial photograph capture; the Ridge Line, defined as the point of highest elevation on the supra-tidal beach; and the Vegetation Line, defined as the point of transition between the beach and landward vegetation. The shoreline obtained from LiDAR DEMs is a datum-based MHWL calculated from a 19-year record (1997-2016) at Cromer tide gauge. In total, the combination of data sources and shoreline definitions resulted in 67 digitized shorelines spanning the period 1886 to 2016 (Table 1).

Shoreline definition	**Time period**	**Data source**	**Frequency**
Mean High Water Line	1886 - 2016	Historical maps	1886; 1905; 1928*; 1957*; 1981*; 2016
High Water Line	1992 - 2016	Vertical aerial photography	1992; 1994; 1997; 2001; 2003; annual thereafter
Ridge Line	1992 - 2016	Vertical aerial photography	1992; 1994; 1997; 2001; 2003; annual thereafter
Vegetation Line	1992 - 2016	Vertical aerial photography	1992; 1994; 1997; 2001; 2003; annual thereafter
Mean High Water Line	2003 - 2015	LiDAR	2003; 2006; 2008; 2011^{+}; 2013^{+}; 2014; 2015

*Table 1: Summary of extracted shorelines. *obtained from Digimap historic roam. $^{+}$downloaded as DSMs, all other LiDAR datasets are DTMs at between 2 and 0.25 m resolution.*

2.2 Shoreline extraction

The procedures required to extract shorelines varied depending on the data source and associated shoreline definition.

To check for tears, creases, or shrinkage, historical maps were inspected in hardcopy before being digitized and georeferenced (Moore, 2000). Once imported to GIS, the MHWL was vectorized automatically, with the resulting vector drawn down the centre of the mapped MHWL. For the most part, the shoreline represents a distinct, linear feature that is easily distinguished from the background resulting in accurate automated extraction. The presence of text and other linear features (such as the Mean Low Water Line) meant that in all instances, some manual tidying was required to ensure a single continuous shoreline was produced.

The HWL and Vegetation Line proxies were predicated on visually discernible differences in pixel values. To improve extraction, vertical aerial photographs were enhanced using both vertical and horizontal Sobel convolution functions (Pollard et al., 2019a). This procedure emphasized contrast between pixel values. The enhanced image was then converted to a bitonal image, enabling shoreline vectorization in a semi-automated fashion, reducing the subjectivity that would have been introduced through purely manual extraction. As shown in Figure 1C, the vegetation type is variable alongshore, with dune vegetation persisting at the western terminus, salt marsh towards the middle sections, and grazing marsh at the eastern end. The Ridge Line does not have such a distinct visual representation but is characterized by a clear elevation signal. As the UK Environment Agency undertakes regular bi-annual 'winter' and 'summer' cross-shore profiling (for locations see Figure 1C) in this area, Ridge Line extraction from the vertical aerial photography was cross-checked against the closest time-matched cross-shore topographic survey.

For the LiDAR-derived MHWL, the water level was first calculated based on a 19-year time series of tidal water levels using the Cromer tide gauge. This is necessary to remove the nodal tidal signal and is standard practice in shoreline change assessment (Hapke et al., 2011; Robertson et al., 2004). Water level values were adjusted to account for the tidal slope (based on the difference in Mean High Water Springs between Cromer and Hunstanton (Christie et al., 2018) between Blakeney Point and the Cromer gauge location. Following Farris et al. (2018), the calculated MHWL of +2.234 m was then contoured onto the LiDAR DEM. To filter out noise introduced by the LiDAR resolution, the contoured MHWL was smoothed using a PAEK (Polynomial Approximation with Exponential Kernel) smoothing algorithm with a smoothing window of 10 m (Farris et al., 2018).

2.3 Shoreline positional error

Three sources of shoreline positional error were quantified through reference to Sutherland's (2012) equation:

$$RMST = \sqrt{RMSS^2 + RMSI^2 + RMSV^2} \quad \text{(Equation 1)}$$

where RMST = root-mean-square total error, RMSS = root-mean-square source error, RMSI = root-mean-square interpretation error, and RMSV = root-mean-square variability error. RMSS error is the accuracy of a point compared to its actual location on the ground (Moore, 2000). RMSI error quantifies the error introduced by the surveyor in their interpretation of where the shoreline lies (Moore, 2000). RMSV error is a measure of the horizontal variability in the cross-shore position of a given contour, due to natural changes in the waves, currents and water levels (Sutherland, 2012). Equation 1 was used to calculate total error associated with each of the 67 shorelines. The measurement of each error term varies by shoreline proxy (Table 2).

Shoreline proxy	RMSS	RMSI	RMSV
Mean High Water Line (Historical maps)	*Geo-referenced against 2016 Ordnance Survey 1:1000 Master map	Standard error values calculated by Sutherland (2012) were used to account for the following vertical errors: i. error in the tide table level; ii. difference between predicted and surveyed water level; iii. variation in water level either side of the peak water level; and iv. variation in tideline position due to wave set-up and swash. Vertical errors were converted to horizontal errors using an estimate of beach slope derived from cross shore topography surveys. Semi-automated vectorisation was applied, rather than manual tracing from map sheets.	Beach profile variability calculated from cross-shore topography surveys at 0.25 m either side of the MHWL. Variability values were calculated over two periods, 1992-2005 and 2006-2016 to reflect contrasting management regimes. The period 1992-2005 was applied to all shorelines extracted from maps surveyed during the period of active management.
High Water Line	Geo-referenced against 2016 vertical aerial image	*Tide gauge and weather stations consulted to check high tide water level at time of photograph capture. Intersection between high tide water level and cross-shore profiles checked against visible wet/dry line on the vertical aerial photograph. Semi-automated vectorisation applied.	Beach profile variability calculated from cross-shore topography surveys at 0.25 m either side of the MHWL. Variability values were calculated over two periods, 1992-2005 and 2006-2016 to reflect contrasting management regimes
Ridge Line	Geo-referenced against 2016 vertical aerial image	*Visual representation of the Ridge Line on the aerial photograph compared to cross-shore topography surveys.	The Ridge Line is not dependant on a water datum and is a relatively immobile feature resulting in a negligible variability error.

Vegetation Line	Geo-referenced against 2016 vertical aerial image	*At regular alongshore spacing, the envelope between complete sediment and complete vegetation coverage measured manually. Semi-automated vectorisation applied.	The Vegetation Line is not dependant on a water datum and given its landward position on the beach and ecological make-up, is considered a relatively immobile feature resulting in a negligible variability error.
Mean High Water Line (LiDAR)	Horizontal and vertical geo-referencing error taken from EA metadata	*At regular alongshore spacing the deviation between the original and smoothed contour measured.	Beach profile variability calculated from cross-shore topography surveys at 0.25 m either side of the MHWL. Variability values were calculated over two periods, 1992-2005 and 2006-2016 to reflect contrasting management regimes

*Table 2: Error terms for each of the shoreline proxies. The greatest contributor to RMST error for each shoreline proxy is indicated by *.*

Each of the error terms in Table 2 were quantified for each of the 67 shorelines at an alongshore spacing determined by the availability of cross-shore profiles, which varied from 1 km to 200 m, depending on year. The mean error estimates for each error term and shoreline proxy are presented in Table 3.

Shoreline proxy	Mean error (m)			
	RMSS	RMSI	RMSV	RMST
Mean High Water Line (Historical maps)	2.65	1.09	0.13	3.00
High Water Line	0.64	4.65	0.12	4.77
Ridge Line	0.64	7.03	0.00	7.13
Vegetation Line	0.64	1.14	0.00	1.31
Mean High Water Line (LiDAR)	0.43	0.96	0.13	1.09

Table 3: Summary of errors by shoreline proxy.

2.4 Shoreline change analysis

Shoreline change analysis was performed using the open source R-package, Analysing Moving Boundaries Using R (AMBUR) by casting 2064 shore-normal transects along the 10.32 km study frontage at 5 m alongshore spacing (Jackson et al., 2012). Transects were filtered using the inbuilt AMBUR function and then inspected visually to ensure that transects did not cross one another before intersecting the shorelines. The AMBUR package became unstable when analysing the Vegetation Line shorelines, likely due to the complexity of these shorelines, so the Digital Shoreline Analysis System (DSAS; Thieler et al., 2017) v4.4 was used in ArcMap to calculate Vegetation Line changes. An identical transect shapefile was used for both the AMBUR and DSAS analyses, ensuring comparability between the two methods used.

3. Results

Total shoreline change and shoreline change rates for each of the shoreline proxies, covering the entire period of investigation, are presented in Table 4. Over the 130-year period, Blakeney Point has, on average, retreated in a landward direction. The mean retreat rate of -0.60 m a^{-1} is similar to that recorded by the HWL and Ridge Line over the past 24 years but deviates markedly from the rates calculated for both the LiDAR-derived MHWL and the Vegetation Line (Table 4).

		Historical Maps (1886 – 2016)	Vertical Aerial Photography (1992 – 2016)			LiDAR (2003 – 2015)
		Mean High Water Line	HWL	Ridge Line	Vegetation Line	Mean High Water Line
Total change (m)	Mean	-77.63	-14.56	-13.49	-21.93	-2.37
		(-74.63 to -80.63)	(-9.79 to -19.33)	(-6.36 to -20.62)	(-20.62 to -23.24)	(-1.28 to -3.46)
	Median	-106.64	-16.82	-14.12	-14.25	-3.19
		(-103.64 to -109.64)	(-12.05 to -21.59)	(-6.99 to -21.25)	(-12.94 to -15.56)	(-2.10 to -4.28)
	Standard Deviation	75.63	15.78	11.63	27.57	8.66
Change rate ($m\ a^{-1}$)	Mean	-0.60	-0.61	-0.57	-0.92	-0.19
		(-0.58 to -0.62)	(-0.41 to -0.81)	(-0.27 to -0.87)	(-0.87 to -0.97)	(-0.10 to -0.28)
	Median	-0.82	-0.71	-0.59	-0.60	-0.26
		(-0.80 to -0.84)	(-0.51 to -0.91)	(-0.29 to -0.89)	(-0.55 to -0.65)	(-0.17 to -0.35)
	Standard Deviation	0.58	0.66	0.49	1.16	0.70

Table 4: Summary of total shoreline change and shoreline change rates for five shoreline proxies from three data sources. Revised from Pollard et al., 2019b. Mean RMST error bands were applied to each shoreline proxy and are shown in brackets.

Figure 2 shows the mean annual shoreline change rate for the HWL, Ridge Line, and Vegetation Line for the period 1992-2016 (dashed line) and for each year within this period for which a shoreline was available (solid line). The equivalent shoreline change rates for LiDAR and historical map derived MHWL are shown over the periods 2003-2015 and 1886-2016 respectively. The height of the grey shaded box in Figure 2 indicates the RSMT error associated with each shoreline proxy and the width indicates the timescale required for the mean shoreline change rate to exceed the RMST error (Table 3). Accordingly, the HWL Figure 2A), Ridge Line (Figure 2B), and Vegetation Line (Figure 2C) require 8, 13, and 2 years of mean shoreline change to exceed their respective error terms. The LiDAR-derived MHWL (Figure 2D) and historical map-derived MHWL (Figure 2E) require 6 and 5 years of mean change to exceed their respective error terms.

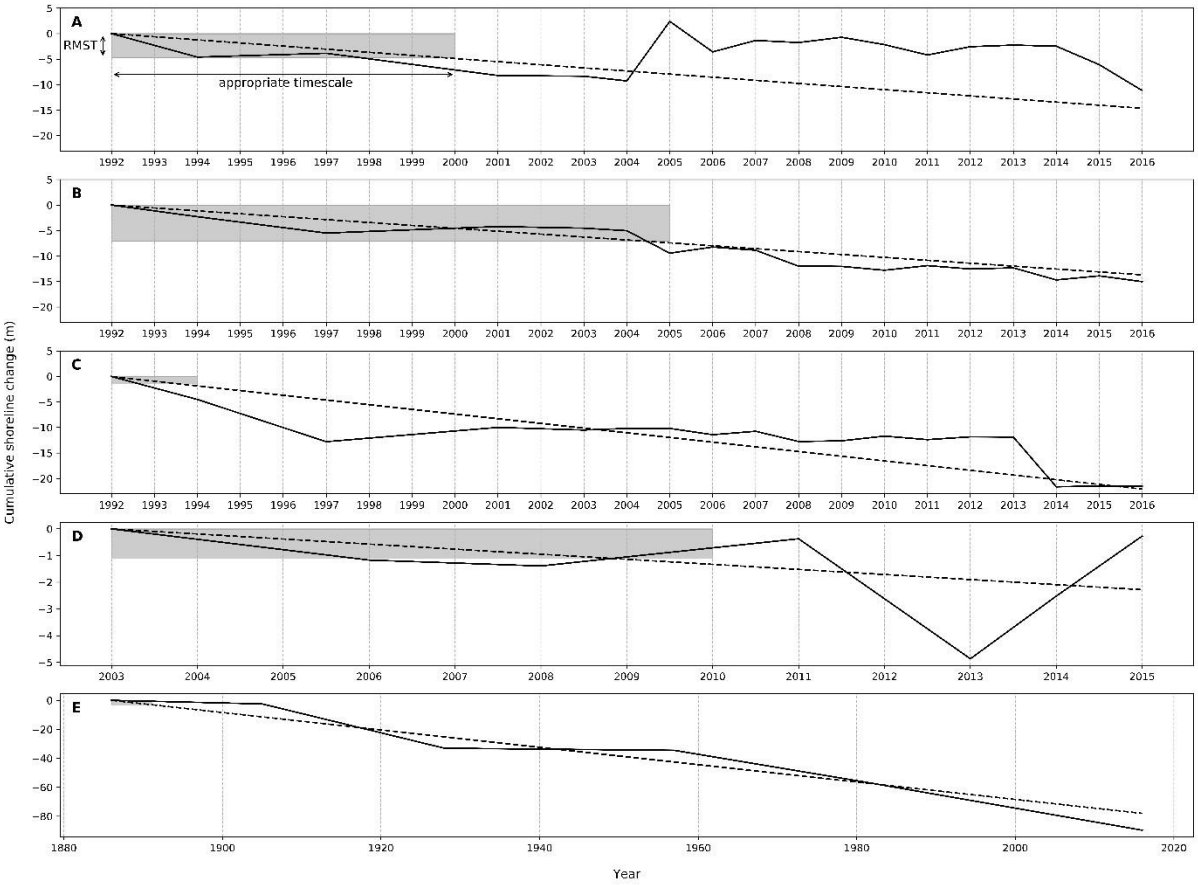

Figure 2: Comparison of cumulative shoreline change and RSMT error for HWL (A), Ridge Line (B), Vegetation Line (C), LiDAR-derived MHWL (D) and historical map-derived MHWL (E) proxies. The dashed line indicates the mean shoreline change calculated over the entire period shown; the solid line indicates the shoreline change calculated year on year. Grey boxes indicate RMST errors and appropriate timescales for calculation of shoreline change statistics for each proxy. Note that panels A, B, and C share common axes and panels D, and E differ in both x- and y- axes.

The bulk statistics in Table 4 do not capture alongshore variations in retreat rates. Figure 3A shows that landward retreat has dominated over most of the spit's length between 1886 and 2016, reaching a maximum of 146 m at the spit's midpoint, seawards of Cley (Figure 1C). High rates of horizontal accretion, of up to 351 m, have characterized the western end of Blakeney Point. Figure 3B maps shoreline change rate (enabling comparability between unevenly spaced map dates) for a series of time intervals within the 130-year timespan. The periods 1886-2016, 1905-2016, and 1957-2016, clearly show a tendency towards accretion of the western section, with a maximum shoreline advance rate at a single transect of up to 2.70 m a^{-1}, 2.90 m a^{-1}, and 2.00 m a^{-1} respectively. Over the same periods, every transect in the eastern section was in retreat, with a maximum shoreline retreat rate at a single transect of up to -0.64 m a^{-1}, -0.74 m a^{-1}, and -0.62 m a^{-1} respectively. This contrasts markedly with the period 1981-2016 where no transects displayed accretion and minimum shoreline retreat rates of -0.32 m a^{-1} and -0.35 m a^{-1} was recorded along the western and eastern sections respectively.

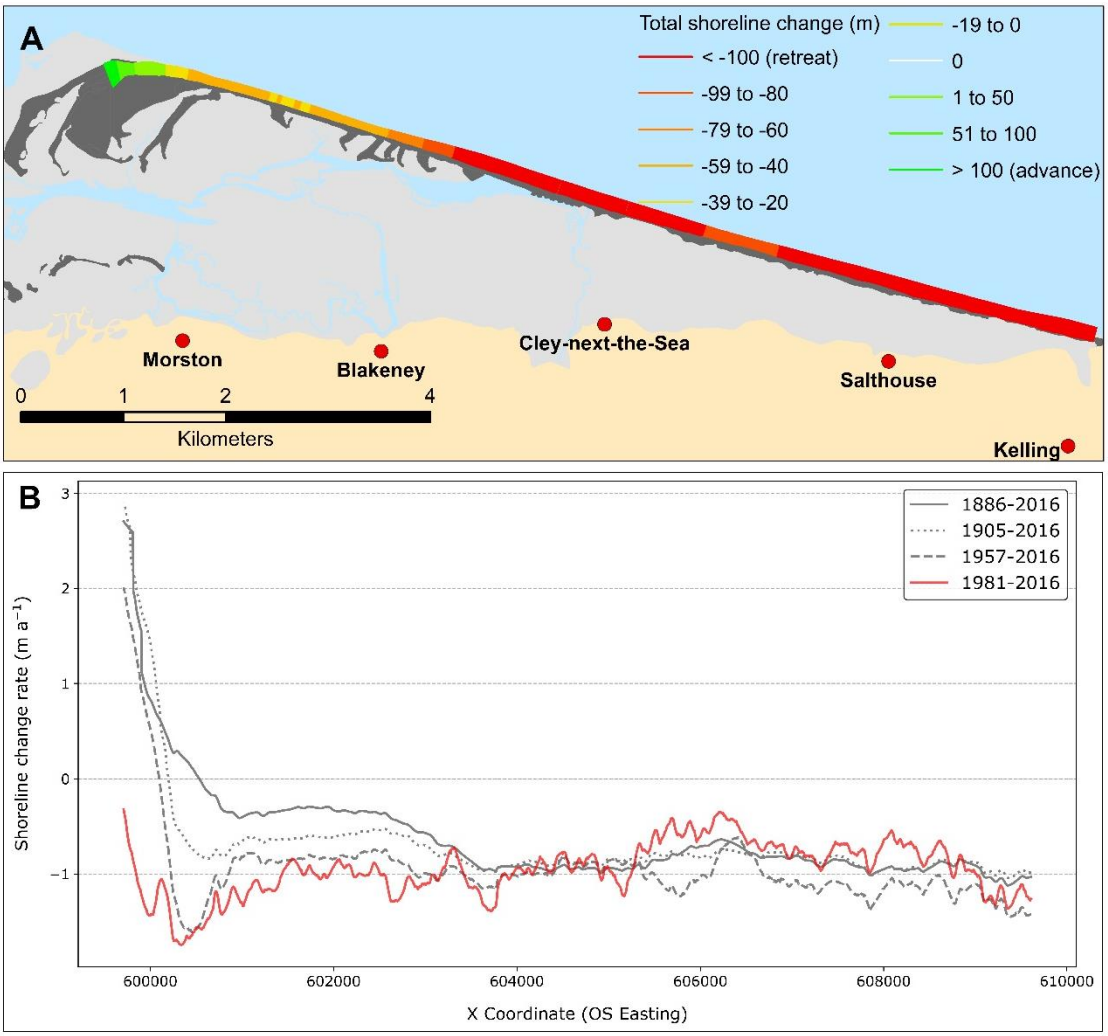

Figure 3: Shoreline changes from historical map derived MHWL. A: Total shoreline change in planform, 1886-2016. B: Shoreline change rate over the period of record and disaggregated

into four variable length, multi-decadal timespans. Only shorelines covering the entire spit extent are shown (hence the absence of the 1928 shoreline).

The HWL, Ridge Line and Vegetation Line proxies are available for the period 1992-2016. This period can be subdivided into a managed era (1992-2005), during which time the spit east of Cley was periodically reprofiled (Figure 1C), and an unmanaged era (2006-2016), during which time the entire spit was not managed actively. Figure 4 shows histograms for each proxy available over this period, separated into western (never actively managed) and eastern (actively managed during the period 1992-2005) sections for the two eras described above.

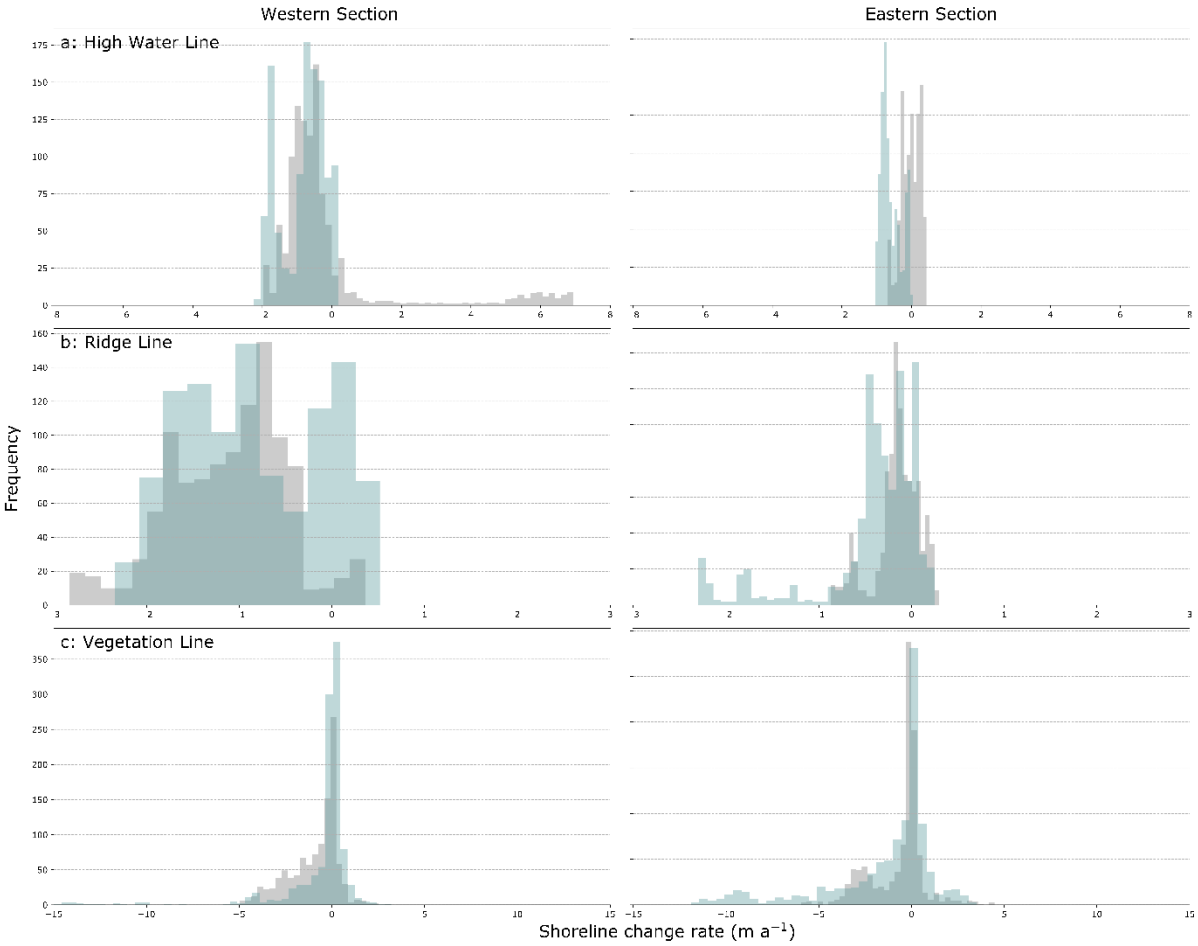

Figure 4: Shoreline change rate histograms for the HWL (A), Ridge Line (B) and Vegetation Line (C) proxies categorised by section (left column: western; right column: eastern) and management regime eras (shaded: managed era, 1992-2005; crosshatched: unmanaged era, 2006-2016). Note that x and y axes vary between panels A, B, and C.

Figure 4A shows HWL shoreline change along the western and eastern sections respectively. The western section was dominated by retreat in both eras, though with some instances of high accretion rates during the managed era. The eastern section shows distinctly different behaviour when comparing the two eras. During the earlier managed era, the eastern section was relatively more stable, with high frequencies around 0 m of shoreline change, while in

the unmanaged era, this section experienced only shoreline retreat. For the Ridge Line (Figure 4B), the western section showed higher frequency of retreating profiles in the managed era than the unmanaged era. However, the eastern section displayed the opposite behaviour, with higher shoreline retreat during the unmanaged era. The Vegetation Line (Figure 4C) was relatively more stable regardless of section or era, compared to the HWL and Ridge Line, with a greater frequency of profiles around 0 m of shoreline change Despite this overall stability, there was a marked increase in the frequency of negative transects in the eastern section during the unmanaged era.

Research into barrier morphodynamics suggests that barrier response to extreme hydrodynamic events may contribute significantly to shoreline changes observed at coarser temporal resolution (Masselink and Van Heteren, 2014; Orford et al., 1996). Furthermore, the societal impacts of extreme hydrodynamic events means that their timing and characteristics are often well-documented (e.g. Garnier et al. (2017) and Haigh et al. (2017)). Table 5 reports storm events since 1992 that are known to have had a substantial societal impact on the North Norfolk coast (Brooks et al., 2016). Total shoreline change calculated from vertical aerial photographs either side of each event (and in some cases two events) are shown for the HWL, Ridge Line and Vegetation Line. Based on the magnitudes of change and proxy-dependant RMST error (Table 3), only the Vegetation Line detects discernible coastal change over a single year.

Event(s)	**Vertical aerial photographs**	**Total shoreline change (m)**		
		HWL	**Ridge Line**	**Vegetation Line**
20 February 1993	1992-1994	-4.73	-2.35	-4.62*
1 January 1995 & 19 February 1996	1994-1997	0.76	-3.26	-8.40*
14 December 2003	2003-2004	-1.08	-0.59	0.38
1 November 2006 & 17 March 2007	2006-2007	2.52	-0.71	0.76
8 November 2007	2007-2008	-0.36	-2.64	-1.70*
5 December 2013	2013-2014	-0.22	-2.49	-10.26*

*Table 5: Significant storm events since 1992 (from Brooks et al., 2016) with pre- and post-event vertical aerial photography, and photograph-derived mean shoreline change for the HWL, Ridge Line and Vegetation Line. Shoreline change figures that exceed RMST error (see Table 3) are indicated with *.*

The Vegetation Line for each of the four storms that recorded total shoreline change greater than the RMST error are mapped in Figure 5. The location and nature of Vegetation Line set-back differs between the earlier and later pairs of storms. For the 1993 and 1995/1996 storms, in addition to some overwashing of the Cley-Salthouse barrier (Figure 5C), a relatively continuous stretch of shoreline retreat occurred on the western section of the barrier (Figure 5B). This behaviour was not observed in the 2007 and 2013 storm events (Figure 5D), where Vegetation Line retreat occurred predominantly as overwashing (and breaching in the case of 2013) of the Cley-Salthouse barrier (Figure 5E).

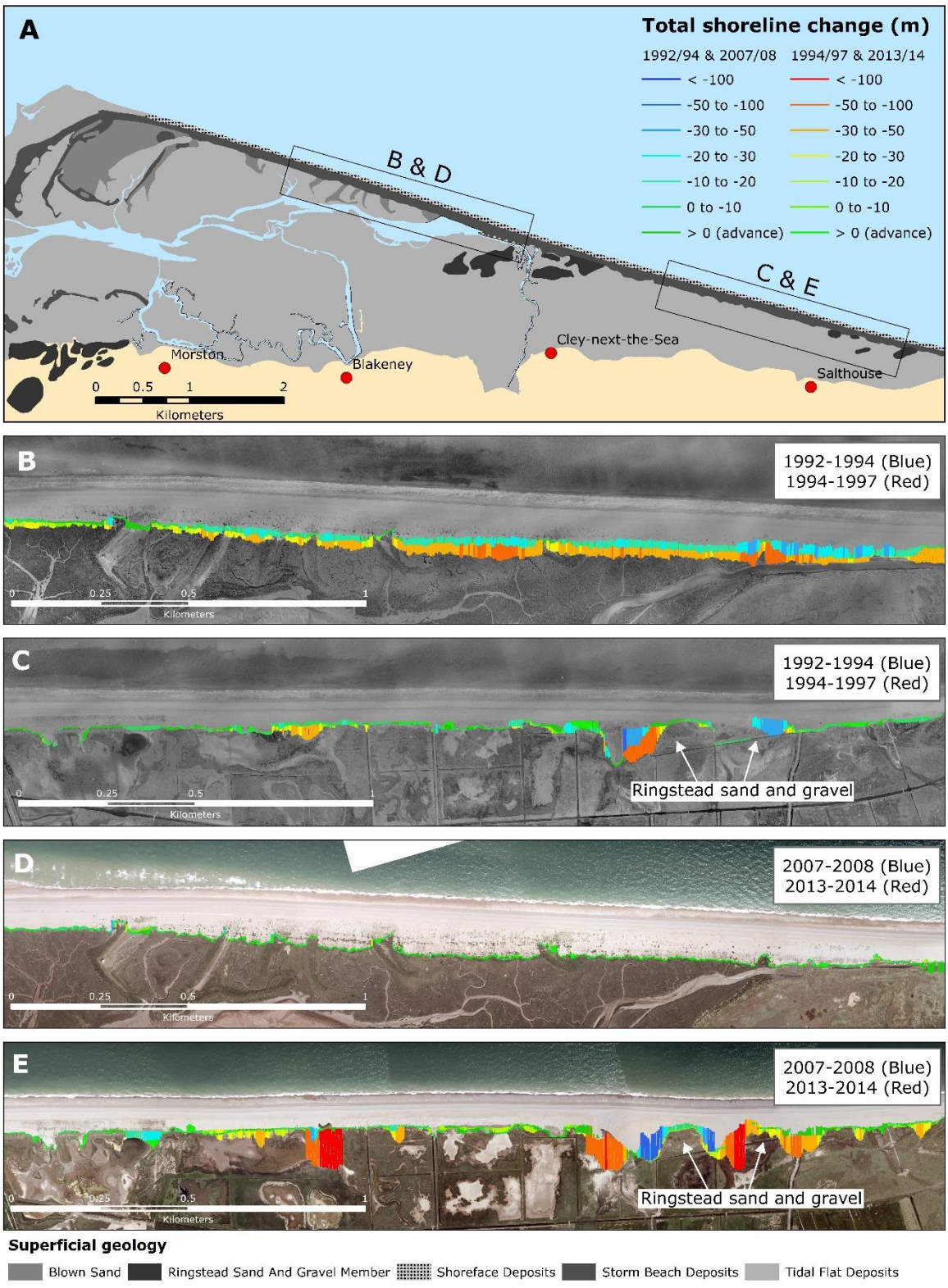

Figure 5: Vegetation Line change for four coastal storms over the period 1992-2016. Two sections of Blakeney Point are displayed for each storm, an eastern section (B and D) and a western section (C and E). Total shoreline change for 1992/94 and 2007/08 are shown in blue shades while red shades are used for the 1994/97 and 2013/14 storms.

4. Discussion

4.1 Appropriate timescales for shoreline change analysis

The value of shoreline change analysis to coastal management, combined with increasing availability of data sources from which shorelines can be extracted, raises important methodological issues. Meaningful shoreline analysis requires genuine shoreline change to be distinguished from the errors introduced by the originating datasets and subsequent definition and extraction procedures (Boak and Turner, 2005; Camfield and Morang, 1996; Moore, 2000; Thieler and Danforth, 1994). If shoreline changes lie within the error bounds of the shoreline position, it is not possible to assert directional shoreline change. By considering proxy-specific shoreline change alongside their associated error terms (Figure 2), it is possible to calculate appropriate timescales over which shoreline changes can be considered distinct from associated error (Thieler and Danforth, 1994).

In this study at annual timescales, shoreline change rate varied substantially about the mean trend. Based on the RMST errors calculated in this study, during phases of greater shoreline change, shorter time periods of observation were sufficient to separate the shoreline signal from the associated error. For example, for the period 2004-2005, the HWL experienced a total shoreline change of 11.60 m, more than double the associated error of 4.77 m. Over the period 2013-2014, the Vegetation Line change of 9.75 m exceeded the associated error of 1.31 m by seven times, representing a clear shoreline change signal. The importance of relative difference between shoreline signal and error is well demonstrated by comparing the LiDAR-derived MHWL and the Vegetation Line. Despite the LiDAR-derived MHWL having the lower RMST of the two shoreline proxies, over double the monitoring period length is required to detect discernible change compared to the Vegetation Line. This arises because of the lower magnitude of total shoreline change detected by the LiDAR derived MHWL compared to the Vegetation Line.

Because different shoreline proxies encode varying levels of error, appropriate timescales for shoreline change analysis become proxy-specific. These appropriate timescales are dependent on both the shoreline associated error and the magnitude of shoreline change that is measured. Rather than dismissing shoreline proxies with relatively higher error terms, it is possible to draw robust conclusions from shoreline change calculated over longer periods where the shoreline signal can be considered distinct from the noise. This ensures that insights from alternative shoreline proxies are not dismissed out of hand, leading to a richer understanding of coastal dynamics in any given locality. It is important to recognise that the error terms associated with any one of the shoreline proxies analysed in this study are likely to differ depending on the coastal environment in which they are found. For example, in hyper arid coastal environments, the Vegetation Line may be highly discontinuous and or influenced by seasonal weather patterns resulting in increased variability error (Pollard et al., 2019a). Alternatively, in soft-cliffed coastal environments, the Vegetation Line may coincide with a cliff edge resulting in increased interpretation and variability error associated with cliff

slumping or collapse (Brooks and Spencer, 2010). Rather than the error terms themselves, it is the procedures involved in determining appropriate timescales for shoreline change analysis that should be applied to other coastal environments.

Critical attention towards relative magnitudes of shoreline signal and noise assume renewed relevance in the context of satellite-derived shorelines which, owing to the resolution of images from which they are derived and the global extent of their application, are associated with relatively higher error terms (e.g. Luijendijk et al., 2018; Vos et al., 2019). Satellite imagery is available from the 1970s, enabling shoreline change calculations over multidecadal timescales in coastal environments characterised by more subtle shoreline change signals. Obviously in locations where shoreline changes are more dramatic, appropriate timescales for shoreline change analysis will be shorter, perhaps even sub-annual (see Vos et al., 2019). Furthermore, continuously improving resolution of satellite imagery can be expected to reduce the timescales required to detect discernible shoreline change in the future.

Quantifying the error associated with shoreline definition and extraction is a necessary, but not sufficient, procedure. This study considers the relative difference between shoreline change and associated error to guide subsequent selection of appropriate time periods over which to conduct shoreline change analysis for each of the shoreline proxies. The time periods used for shoreline change analysis satisfy the condition that shoreline change exceeds the associated shoreline positional error on a proxy-by-proxy basis. This proxy-specific approach is preferable when compared to generic approaches, which vary considerably between studies (Boak and Turner, 2005). For instance, while Eliot and Clarke (1989) recommend at least 10 years of continuous records to distinguish shoreline change trends from short term variability, Galgano and Leatherman (1991) advocate for records exceeding 50 years. Accounting for error in this way enables greater confidence when attributing coastal processes to the observed shoreline changes.

4.2 Shoreline proxies and associated processes

Deploying a multi-proxy approach over centennial to event timescales ensures that different cross-shore locations are captured. The concomitant processes are specific, to some extent, to the coastal setting of Blakeney Point and its particular hydrodynamic, meteorological, ecological and human influence contexts. Yet, differences in cross-shore position can be more generally interpreted as points along a continuum of marine-to-terrestrial process controls, a feature common to the full diversity of coastal environments. As such, the process understanding obtained here is richer in detail, capturing interactions between processes that dominate at different cross-shore locations, as a result of a multi-proxy approach.

Centennial shoreline dynamics provide insights into trends in shoreline position, landform persistence and long-term habitat viability. At Blakeney Point, the historical map derived MHWL revealed a mean shoreline retreat of -0.60 m a^{-1} over the 130 year period between

1886-2016. The median total shoreline change over the period 1886-2016 was nearly 40% greater than the mean value, suggesting that a small number of highly accretionary profiles influenced the mean shoreline change figure (Table 4). The skewing of the mean towards less negative values can be explained by the accretion towards the western end of Blakeney Point and the persistence of drift alignment over the period 1886-1981 (Figure 3A). Shoreline retreat dominated the central and eastern section of the spit, with maximum mean annual retreat rates of 1.16 m. This behaviour, termed 'cannibalisation', is a hallmark of drift-aligned gravel barrier systems (Bujalesky and Bonorino, 2015; Orford et al., 1991). The sediment-limited nature of such systems means that continued accretion of downdrift sections occurs at the expense of those located updrift. Figure 3B reveals the most recent interval, 1981-2016, did not follow the centennial trend and rather, suggests a shift towards a more swash-aligned system. According to conceptual models of gravel barrier evolution (Carter et al., 1987; Orford et al., 1996), swash-aligned systems are more vulnerable to overwashing and landward retreat during storms. Continued vulnerability to storm events increases the potential for barrier breakdown if barrier elevation is reduced sufficiently for widespread breaching to occur.

Over the 24-year period spanning 1992-2016, annual vertical aerial photography enabled extraction of the HWL, Ridge Line, and Vegetation Line shoreline change proxies (Table 4). Deriving a mean annual rate of shoreline change allowed comparability between multi-decadal periods of analysis and comparison to the centennial record. The HWL and Ridge Line were relatively invariant alongshore with mean retreat rates of -0.61 m a^{-1} and -0.57 m a^{-1} respectively over the past 24 years; similar to that recorded by the historical map derived MHWL (-0.60 m a^{-1}) over the past 130 years. This mean shoreline retreat figure for Blakeney Point equates to the -0.61 m a^{-1} estimated by Hunter and Mottram (1925) based on the movement of the lee fringe and crest relative to a series of telephone pole markers. The values obtained in this study are slightly lower than Hardy's (1964) map-derived estimate of -0.91 m a^{-1} over the period 1905-1956. Based on the HWL and Ridge Line proxies, it appears that the evolution of Blakeney Point in recent decades corresponds well with the centennial trend.

When the Vegetation Line is considered, however, this interpretation breaks down. The Vegetation Line showed large deviations between the median (-0.60 m a^{-1}) and mean (-0.92 m a^{-1}) shoreline change figures, an indication of high alongshore variability in shoreline change rates. Furthermore, the mean Vegetation Line retreat was 50 % greater than the HWL, Ridge Line and the centennial trend. During the four periods mapped in Figure 5, the maximum retreat along a single transect for the Vegetation Line was 60.85 m, 80.76 m, 73.62 m, and 172.98 m respectively, far exceeding the corresponding centennial means. Matching of the hydrodynamic and meteorological record (Table 5) alongside corresponding vertical aerial imagery shows that the observed Vegetation Line setback can be attributed to storm surge events, which result in overwash (Figures 2C, 5C and 5E) and more spatially coherent

sections of retreat (Figure 5B and 5D). Owing to its location towards the landward limit of the beach profile, the Vegetation Line is effective at recording and preserving extreme event impacts. Locations closer to mean sea level on the beach profile are more exposed to post-event recovery processes (Brooks et al., 2017; Lazarus et al., 2019) making the morphological impact of storm surge events difficult to isolate when vertical aerial photographs are only captured annually. Landward rollover of the Cley-Salthouse barrier during storm surges has long been identified as one of the key forms of sediment movement at Blakeney Point (Clymo, 1967); following the storm surge of 31 January – 1 February 1953, Steers and Grove (1953) estimated an average barrier rollover of 27-37 m.

However, when calculated as a mean annual rollover rate, the retreat of the Cley-Salthouse barrier based on the Vegetation Line has been less, at 0.91 m a^{-1}, than rates recorded for barriers elsewhere (e.g. at Story Head, Nova Scotia which retreated at 8 m a^{-1} following a substantial reduction in volume (Forbes et al., 1991)). The relatively slower retreat of the Cley-Salthouse barrier may derive from the developed back-barrier salt marsh, and in places reclaimed marsh, and consequent reduction of tidal prism; both of which have been observed to grant stability to fronting gravel barriers (Long et al., 2006). The presence of developed back-barrier salt marsh elsewhere, in combination with other characteristics, such as beach materials and associated beach gradients that reflect incident wave energy, has led to suggestions that barriers represent comparatively resilient coastal landforms (Kombiadou et al., 2019; Masselink and Lazarus, 2019). Superficial geology (Figure 5A) also likely plays a role by moderating breach and overwash location. Over individual storm surge impacts, the presence of Ringstead Sand and Gravel outcrops at the shoreline (Morelock et al., 2008) – locally known as 'eyes' - are associated with lower rates of Vegetation Line set-back but encourage, presumably through influencing patterns of wave refraction, increased rates of shoreline retreat at their margins (Figure 5E). Over multi-decadal timescales, the presence of outcrops of these more resistant gravel deposits may contribute to increased barrier inertia, resulting in 'sticking points' characterised by reduced shoreline retreat (Orford et al., 2002). However, over centennial scales, there is little evidence that alongshore variability in shoreline retreat rates may promote the breakdown of the barrier itself, as has been suggested elsewhere (Environment Agency, 2010).

Finally, that certain proxies capture certain processes is further supported by the LiDAR-derived MHWL, which recorded total shoreline change and change rates that were, at most, 30% less than those recorded by the other four shoreline proxies. The relatively low retreat rates (0.19 m a^{-1}) recorded by the LiDAR derived MHWL are possibly explained by the cross-shore position which, at +2.234 m, is the lowest and most seaward of the proxies analysed here. It follows that this shoreline will be most likely to undergo redistribution of sediment in response to daily inundation and exposure to wave breaking. It is also likely to be the steepest point on the cross-shore profile and so subject to the most reflective conditions with resultant swash asymetry providing an effective mechanism for resisting substantial shoreline change

(Buscombe and Masselink, 2006; Masselink and Puleo, 2006). The limited nature of shoreline dynamics captured by the LiDAR-derived MHWL emphasises the value of extracting alternative shoreline proxies.

4.3 Shoreline proxies, management regime and spatial variability in barrier response

A key strength of extracting multiple shoreline proxies is the ability to investigate relative movement on different parts of a barrier system. At Blakeney Point, the histograms shown in Figure 4 reveal disparate responses of the HWL, Ridge Line and Vegetation Line to the cessation of active reprofiling of the eastern section of Blakeney Point in winter 2005. Figure 4B shows Ridge Line change along the western and eastern sections respectively. The higher frequency of large shoreline retreat rates during the managed era in the western section likely represents sediment starvation resulting from the active reprofiling of the updrift eastern section. This assertion is also supported by the relatively higher rates of retreat experienced by the eastern section during the unmanaged era. The increase in retreat rate of the eastern section appears to have been releasing sediment to be transported downdrift, resulting in buffering and reduced shoreline retreat in the western section. Figure 4A suggests that active reprofiling of the barrier ridge had impacts lower down the beach profile. During the managed era, the HWL displayed greater stability whereas during the unmanaged era, the modal frequency was concentrated at greater than 1 m a^{-1} of shoreline retreat. During the period of active management, re-profiling represented a dominant external forcing factor preventing the more natural barrier response to storms observed after the termination of re-profiling (Figure 4B). Reprofiling led to the positional stability of the barrier, particularly the Ridge Line, maintained by artificial means. The termination of re-profiling resulted in substantial morphological changes as the barrier was set on a trajectory towards the alternative (but also stable) attractor state of landward rollover (Carter and Orford, 1993).

5. Conclusions

Rather than seeking to establish the 'most accurate' approach to shoreline change analysis on gravel barrier systems, this study has emphasised the value of extracting multiple shoreline proxies in the recognition that each makes a unique contribution to explaining morphological changes at different locations on a barrier system over centennial to event timescales. There is a fundamental interdependence between choice of shoreline proxy and the coastal processes that are observed. The ability to extract a variety of shoreline proxies depends on the availability of data sources, the characteristics of the coastal setting in question, and the intended outcomes of research. For instance, the analysis conducted here benefited from historic mapping efforts, quasi-continuous instrument wave buoys, tide gauge records, and an established field and remote sensing monitoring campaign conducted by the UK Environment Agency. It is important, once a range of shoreline proxies have been extracted, to undertake a rigorous quantification of associated sources of error, with comparison against observed proxy-specific shoreline change rates. Appropriate timescales for shoreline change analysis need to be established for each derived shoreline proxy. Using the appropriate

timescales to guide subsequent shoreline change analysis ensures that the observed shoreline changes can be considered distinct from the error associated with shoreline definition and extraction procedures. Finally, shoreline change analysis of multiple shoreline proxies provides for detailed understanding of contemporary morphodynamics, in this instance for a mixed sand-gravel spit environment, including response to management regime change and storm surge events.

The diversity of coastal processes captured in this study suggest that using a single shoreline proxy out of ease of extraction, or from the demands of legacy/continuity, runs the risk of narrowing understanding of coastal zones and the internal and external forcing to which they are exposed. This assertion is particularly pertinent given that technological advances (see Viles, 2016) are generating large quantities of data available with potential (though not inevitable) value to the study of coastal systems (Pollard et al., 2018; Rumson et al., 2017). Different datasets lend themselves to certain shoreline definition and extraction procedures. The selection of the MHWL from historical maps, for example, derives solely from the fact that this was the shoreline chosen by the UK's Ordnance Survey. On vertical aerial photography, shoreline proxies with a visually discernible feature are required, whereas to obtain a shoreline from a datum-based approach, such as the generation of a LiDAR DEM, requires a complementary long-term tide gauge record.

Given that each proxy captures a different portion of the cross-shore beach, and covers variable time periods, depth of understanding of coastal processes at any given coastal locality is greatly increased by analysing multiple proxies in concert. For instance, the historical map derived MHWL revealed that Blakeney Point has transitioned from a drift-aligned to swash-aligned state since 1981. According to conceptual models of gravel barrier development (Carter et al., 1987), such a transition may indicate increased vulnerability to overwashing and landward retreat in the future, compared to past behaviour. Given that overwash and retreat of Blakeney Point occurs primarily during storm surge events, an assessment of future vulnerability also necessitates attention towards barrier behaviour during these extreme hydrodynamic events. The Vegetation Line was shown to be an effective proxy for detecting storm driven changes on Blakeney Point. High rates of shoreline change as measured by the Vegetation Line support previous research which suggests that barriers are characterised by rapid event-driven changes interspersed by longer periods of relative stasis (Masselink and Van Heteren, 2014; Orford et al., 1996). In this example, storm response is further complicated by the alongshore variable management regime and superficial geology. The influence of management regime was most notable in the Ridge Line proxy which was artificially stabilised over the period 1992-2005, resulting in subdued shoreline change. Superficial geology, in the form of gravel deposits outcropping at the shoreface appears to have influenced the positioning of washover in the short term despite having a limited impact on the centennial timescales (as illustrated by the historical-map derived MHWL).

The dangers of over-reliance on shoreline proxies that are easier to extract are especially prescient given the rapidly increasing availability of remotely sensed datasets. In the case of Blakeney Point, the LiDAR-derived MHWL was relatively easily obtained given the availability of LiDAR DEMs and tide gauge data. However, as noted above, the nature of shoreline dynamics captured by this shoreline proxy was limited, partly owing to its seaward position on the cross-shore profile and also the comparatively limited temporal coverage of LiDAR data. Similar caution should also be applied to shoreline extraction from satellite datasets, which have led to a number of recent global scale analyses in coastal environments (Luijendijk et al., 2018; Mentaschi et al., 2018; Vos et al., 2019). Presently, the instantaneous land-sea interface is the only shoreline that can feasibly be extracted from satellite data at the global scale. While valuable at a global scale, when an understanding of local scale dynamics is required, attention towards alternative shoreline proxies is likely to reveal important cross-shore and long-shore interactions that will not necessarily be captured at this land-sea interface. There is, therefore, a need for critical attention towards the dependencies that exist between shoreline proxy selection and the processes that can be observed as a result. Improvements in the resolution of remotely sensed imagery and increasing sophistication of shoreline extraction techniques will not eliminate the need for subjective decisions over which shorelines are measured and their suitability for understanding coastal behaviour from local to global scales.

Acknowledgements

This work was funded by the NERC/ESRC Data, Risk and Environmental Analytical Methods (DREAM) CDT, Grant/Award Number: NE/M009009/1. It is also a contribution to the NERC-funded project "Physical and Biological dynamic coastal processes and their role in coastal recovery" (BLUE-coast), Grant Award Number: NE/N015924/1.

Data Availability

The datasets used in this study are summarised in Table 6.

Dataset	Originator	Source	Further guidance
Historical Maps	Ordnance Survey / National Grid	In this study, hard copies were consulted at the University of Cambridge. Digital copies for some years are available from Digimap Historic Roam (https://digimap.edina.ac.uk/)	The value of hard copy historical maps lies in the margins, which conceal a record of survey, publication, and revision dates for each map sheet (Brooks and Spencer, 2010). Survey dates can differ from publication dates by several years, which introduces

			substantial error given the time-critical nature of shoreline change analysis (Oliver, 1996).
Vertical aerial photography	Environment Agency	http://environment.data.gov.uk https://www.channelcoast.org/	Individual, georeferenced tiles are available annually since 2001, with reduced availability before this date since not all the years have been digitised. Over the period 1992-2001 single band (greyscale) photographs were captured, with 3-band (red-green-blue) captured over the period 2001-2010, and a fourth infrared band added in 2011.
Light Detection and Ranging (LiDAR)	Environment Agency	http://environment.data.gov.uk	LiDAR digital elevation models are available as either DTM (digital terrain model) which includes vegetation and other visible structures or DSM (digital surface model) where those features are filtered out.
Cross-shore coastal topography surveys	Environment Agency	https://www.channelcoast.org/	Collected for the period 1992-2016 at Blakeney Point, comprising a summer and winter profile for each year. A minimum of twelve profiles were collected biannually at 1 km intervals along the length of Blakeney Point. In some years, additional profiles were collected resulting in minimum alongshore spacing of 200 m along the spit.

Tide gauge	British Oceanography Data Centre	https://www.bodc.ac.uk/	Sampling frequency for the period 1973-1992 was 60 minutes, increasing to 15 minutes in 1993.
Weather data	British Atmospheric Data Centre	http://data.ceda.ac.uk/badc/weybourne/	The weather station at Weybourne is located 4 km east of Salthouse and includes humidity, temperature, irradiance, wind speed, wind direction and atmospheric pressure are available from 2002 to 2016, collected at hourly intervals.

Table 6: Dataset availability with further details of data originator, source, and contextual guidance to facilitate data use.

References

Ahrens, J., 1990. Dynamic revetments, in: Edge, B.L. (Ed.), Proceedings 22nd Conference on Coastal Engineering. ASCE, Delft, pp. 1837–1850.

Allison, H.M., 1989. The sedimentary history of Scolt Head Island, in: Allison, H.M., Morley, J.P. (Eds.), Blakeney Point and Scolt Head Island. The National Trust, Norwich, pp. 28–32.

Aminti, P., Cipriani, L.E., Enzo, P., 2003. "Back to the beach": converting sea walls into gravel beaches, in: Goudas, C.L. (Ed.), Soft Shore Protection. Kluwer Academic Publishers, pp. 261–274.

Bergillos, R.J., Rodríguez-Delgado, C., Ortega-Sánchez, M., 2017. Advances in management tools for modeling artificial nourishments in mixed beaches. J. Mar. Syst. 172, 1–13. https://doi.org/10.1016/j.jmarsys.2017.02.009

Boak, E.H., Turner, I.L., 2005. Shoreline definition and detection: a review. J. Coast. Res. 21, 688–703. https://doi.org/10.2112/03-0071.1

Bradbury, A.P., Orford, J.D., 2007. Influence of changing management regimes on the morphodynamic response, of a mixed gravel and sand barrier beach, in: Kraus, N.C., Rosati, J.D. (Eds.), Coastal Sediments 2007. ASCE, New Orleans, pp. 1–14. https://doi.org/10.1002/pros.22522

Brooks, S.M., Spencer, T., 2019. Long-term trends, short-term shocks and cliff responses for areas of critical coastal infrastructure, in: Wang, P., Rosati, J.D., Vallee, M. (Eds.), Coastal Sediments 2019. World Scientific, pp. 1179–1187.

Brooks, S.M., Spencer, T., 2010. Temporal and spatial variations in recession rates and sediment release from soft rock cliffs, Suffolk Coast, UK. Geomorphology 124, 26–41. https://doi.org/10.1016/j.geomorph.2010.08.005

Brooks, S.M., Spencer, T., Christie, E.K., 2017. Storm impacts and shoreline recovery: mechanisms and controls in the Southern North Sea. Geomorphology 283, 48–60. https://doi.org/10.1016/j.geomorph.2017.01.007

Brooks, S.M., Spencer, T., McIvor, A., Möller, I., 2016. Reconstructing and understanding the impacts of storms and surges, southern North Sea. Earth Surf. Process. Landforms 41, 855–864. https://doi.org/10.1002/esp.3905

Bujalesky, G., Bonorino, G., 2015. El Paramo transgressive gravel spit, Tierra del Fuego, Argentina, in: Randazzo, G., Jackson, D., Cooper, A. (Eds.), Sand and Gravel Spits. Springer, pp. 37–50. https://doi.org/10.1007/978-3-319-13716-2_3

Burgess, H.M., Kilkie, P., 2015. Understanding the physical processes occurring within a new coastal managed realignment site, Medmerry, Sussex, UK, in: ICE Coastal Management. Institute for Civil Engineers, Amsterdam, pp. 1–14.

Burningham, H., 2015. Gravel spit-inlet dynamics: Orford Spit, UK, in: Randazzo, G., Jackson, D., Cooper, A. (Eds.), Sand and Gravel Spits. Springer, pp. 51–65. https://doi.org/10.1007/978-3-319-13716-2_4

Buscombe, D., Masselink, G., 2006. Concepts in gravel beach dynamics. Earth-Science Rev. 79, 33–52. https://doi.org/10.1016/j.earscirev.2006.06.003

Camfield, F.E., Morang, A., 1996. Defining and interpreting shoreline change. Ocean Coast. Manag. 32, 129–151. https://doi.org/10.1016/S0964-5691(96)00059-2

Carapuço, M.M., Taborda, R., Silveira, T.M., Psuty, N.P., Andrade, C., Freitas, M.C., 2016. Coastal geoindicators: towards the establishment of a common framework for sandy coastal environments. Earth-Science Rev. 154, 183–190. https://doi.org/10.1016/J.EARSCIREV.2016.01.002

Carter, R.W.., Forbes, D.., Jennings, S.., Orford, J.., Shaw, J., Taylor, R.., 1989. Barrier and lagoon coast evolution under differing relative sea-level regimes: examples from Ireland and Nova Scotia. Mar. Geol. 88, 221–242. https://doi.org/10.1016/0025-3227(89)90099-6

Carter, R.W.G., Orford, J.D., 1993. The morphodynamics of coarse clastic beaches and barriers: a short- and long-term perspective. J. Coast. Res. Special Is, 158–179.

Carter, R.W.G., Orford, J.D., Forbes, D.L., Taylor, R.B., 1990. Morphosedimentary development of drumlin-flank barriers with rapidly rising sea level, Story Head, Nova Scotia. Sediment. Geol. 69, 117–138. https://doi.org/10.1016/0037-0738(90)90104-2

Carter, R.W.G., Orford, J.D., Forbes, D.L., Taylor, R.B., 1987. Gravel barriers, headlands, and lagoons: an evolutionary model, in: Kraus, N.C. (Ed.), Coastal Sediments 1987. American Society of Civil Engineers, New York, pp. 1776–1792.

Casella, E., Rovere, A., Pedroncini, A., Stark, C.P., Casella, M., Ferrari, M., Firpo, M., 2016. Drones as tools for monitoring beach topography changes in the Ligurian Sea (NW Mediterranean). Geo-Marine Lett. 36, 151–163. https://doi.org/10.1007/s00367-016-0435-9

Cheong, S.-M., Silliman, B., Wong, P.P., van Wesenbeeck, B., Kim, C.-K., Guannel, G., 2013. Coastal adaptation with ecological engineering. Nat. Clim. Chang. 3, 787–791.

https://doi.org/10.1038/nclimate1854
Christie, E.K., Spencer, T., Owen, D., McIvor, A.L., Möller, I., Viavattene, C., 2018. Regional coastal flood risk assessment for a tidally dominant, natural coastal setting: North Norfolk, southern North Sea. Coast. Eng. 134, 177–190. https://doi.org/10.1016/j.coastaleng.2017.05.003
Clymo, R.S., 1967. Movement of the main shingle bank at Blakeney Point, Norfolk. Trans. Norfolk Norwich Nat. Soc. 21, 3–6.
Cowell, P.J., Stive, M.J.F., Niedoroda, A.W., De Vriend, H.J., Swift, D.J.P., Kaminsky, G.M., Capobianco, M., 2003. The Coastal-Tract (part 1): a conceptual approach to aggregated modeling of low-order coastal change. J. Coast. Res. 19, 812–827.
de Vriend, H., Aarninkhof, S., van Koningsveld, M., 2014. 'Building with nature': the new Dutch approach to coastal and river works, in: Proceedings of the ICE - Civil Engineering. pp. 18–24. https://doi.org/10.1680/cien.13.00003
Defra, 2006. Shoreline management plan guidance Volume 1: Aims and requirements. London.
Dolan, R., Hayden, B., May, P., May, S., 1980. The reliability of shoreline identification from aerial photographs. Shore and Beach 48, 22–29.
Durán, R., Guillén, J., Ruiz, A., Jiménez, J.A., Sagristà, E., 2016. Morphological changes, beach inundation and overwash caused by an extreme storm on a low-lying embayed beach bounded by a dune system (NW Mediterranean). Geomorphology 274, 129–142. https://doi.org/10.1016/j.geomorph.2016.09.012
Duvat, V.K.E., Pillet, V., 2017. Shoreline changes in reef islands of the Central Pacific: Takapoto Atoll, Northern Tuamotu, French Polynesia. Geomorphology 282, 96–118. https://doi.org/10.1016/J.GEOMORPH.2017.01.002
Eliot, I., Clarke, D., 1989. Temporal and spatial bias in the estimation of shoreline rate-of-change statistics from beach survey information. Coast. Manag. 17, 129–156. https://doi.org/10.1080/08920758909362081
Environment Agency, 2014. Sea State Report Norfolk Year 3 and Summary for October 2006 September 2009 (RP039/N/2014). Peterborough.
Environment Agency, 2010. Shoreline Management Plan 5: Hunstanton to Kelling Hard.
Farris, A.S., List, J.H., 2007. Shoreline change as a proxy for subaerial beach volume change. J. Coast. Res. 23, 740–48. https://doi.org/10.2112/05-0442.1
Farris, A.S., Weber, K.M., Doran, K.S., List, J.H., 2018. Comparing methods used by the U.S. Geological Survey Coastal and Marine Geology Program for deriving shoreline position from LiDAR data: U.S. Geological Survey Open-File Report 2018–1121.
Forbes, D.L., Taylor, R.B., Orford, J.D., Carter, R.W.G., Shaw, J., 1991. Gravel-barrier migration and overstepping. Mar. Geol. 97, 305–313. https://doi.org/10.1016/0025-3227(91)90122-K
Fromard, F., Vega, C., Proisy, C., 2004. Half a century of dynamic coastal change affecting mangrove shorelines of French Guiana. A case study based on remote sensing data analyses and field surveys. Mar. Geol. 208, 265–280.

https://doi.org/10.1016/J.MARGEO.2004.04.018
Galgano, F.A., Leatherman, S.P., 1991. Shoreline change analysis: a case study, in: Proceedings of the Coastal Sediments ’91 Conference. American Society of Civil Engineers, Washington, pp. 1043–1053.
Garnier, E., Ciavola, P., Spencer, T., Ferreira, O., Armaroli, C., McIvor, A., 2018. Historical analysis of storm events: case studies in France, England, Portugal and Italy. Coast. Eng. 134, 10–23. https://doi.org/10.1016/j.coastaleng.2017.06.014
Gorelick, N., Hancher, M., Dixon, M., Ilyushchenko, S., Thau, D., Moore, R., 2017. Google Earth Engine: planetary-scale geospatial analysis for everyone. Remote Sens. Environ. 202, 18–27. https://doi.org/10.1016/j.rse.2017.06.031
Grzegorzewski, A.S., Cialone, M.A., Wamsley, T. V, 2011. Interaction of barrier islands and storms : implications for flood risk reduction in Louisiana and Mississippi. J. Coast. Res. Special Is, 156–164. https://doi.org/10.2112/SI59-016.1
Hagenaars, G., de Vries, S., Luijendijk, A.P., de Boer, W.P., Reniers, A.J.H.M., 2018. On the accuracy of automated shoreline detection derived from satellite imagery: A case study of the sand motor mega-scale nourishment. Coast. Eng. 133, 113–125. https://doi.org/10.1016/j.coastaleng.2017.12.011
Haigh, I.D., Ozsoy, O., Wadey, M.P., Nicholls, R.J., Gallop, S.L., Wahl, T., Brown, J.M., 2017. An improved database of coastal flooding in the United Kingdom from 1915 to 2016. Sci. Data 4, 1–10. https://doi.org/10.1038/sdata.2017.100
Hapke, C.J., Himmelstoss, E. a., Kratzmann, M., List, J.H., Thieler, E.R., 2011. National assessment of shoreline change : historical shoreline change along the New England and Mid-Atlantic coasts open-file report 2010 – 1118, U.S. Geological Survey.
Hapke, C.J., Plant, N.G., Henderson, R.E., Schwab, W.C., Nelson, T.R., 2016. Decoupling processes and scales of shoreline morphodynamics. Mar. Geol. 381, 42–53. https://doi.org/10.1016/j.margeo.2016.08.008
Hardy, J.R., 1964. The movement of beach material and wave action near Blakeney Point, Norfolk. Trans. Pap. (Institute Br. Geogr. 34, 53–69.
Harley, J.B., 1975. Ordnance Survey maps: a descriptive manual. Ordnance Survey.
Hill, T.G., Hanley, J.A., 1914. The structure and water-content of shingle beaches. J. Ecol. 2, 21–38.
Hoyt, J.H., 1967. Barrier Island Formation. Geol. Soc. Am. Bull. 78, 1125. https://doi.org/10.1130/0016-7606(1967)78[1125:BIF]2.0.CO;2
Hudson, C., Baily, B., 2018. Delivering sustainable coasts: monitoring the long-term stability of a breached barrier beach, Porlock Bay, Somerset, United Kingdom. Ocean Coast. Manag. 152, 88–99. https://doi.org/10.1016/j.ocecoaman.2017.11.022
Hunter, R.E., Mottram, W.E., 1925. A note on the occurrence of natural preservation of plant tissues. New Phytol. 24, 193–206. https://doi.org/10.1111/j.1469-8137.1925.tb06664.x
Isla, F.., Bujalesky, G.., 2000. Cannibalisation of Holocene gravel beach-ridge plains,northern Tierra del Fuego, Argentina. Mar. Geol. 170, 105–122. https://doi.org/10.1016/S0025-

3227(00)00069-4
Jackson, C.W., Alexander, C.R., Bush, D.M., 2012. Application of the AMBUR R package for spatio-temporal analysis of shoreline change: Jekyll Island, Georgia, USA. Comput. Geosci. 41, 199–207. https://doi.org/10.1016/j.cageo.2011.08.009
Jennings, S., Orford, J.D., Canti, M., Devoy, R.J.N., Straker, V., 1998. The role of relative sea-level rise and changing sediment supply on Holocene gravel barrier development: the example of Porlock, Somerset, UK. The Holocene 8, 165–181.
Kombiadou, K., Costas, S., Carrasco, A.R., Plomaritis, T.A., Ferreira, Ó., Matias, A., 2019. Bridging the gap between resilience and geomorphology of complex coastal systems. Earth-Science Rev. 198, 1–19. https://doi.org/10.1016/j.earscirev.2019.102934
Lazarus, E.D., Harley, M.D., Blenkinsopp, C.E., Turner, I.L., 2019. Environmental signal shredding on sandy coastlines. Earth Surf. Dynam 7, 77–86. https://doi.org/10.5194/esurf-7-77-2019
Long, A.J., Waller, M.P., Plater, A.J., 2006. Coastal resilience and late Holocene tidal inlet history: the evolution of Dungeness Foreland and the Romney Marsh depositional complex (U.K.). Geomorphology 82, 309–330. https://doi.org/10.1016/j.geomorph.2006.05.010
Luijendijk, A., Hagenaars, G., Ranasinghe, R., Baart, F., Donchyts, G., Aarninkhof, S., 2018. The state of the world's beaches. Sci. Rep. 8, 6641. https://doi.org/10.1038/s41598-018-24630-6
Mason, T., Coates, T.T., 2001. Sediment transport processes on mixed beaches: a review for shoreline management. J. Coast. Res. 17, 645–657.
Masselink, G., Lazarus, E.D., 2019. Defining coastal resilience. Water 11, 1–21.
Masselink, G., McCall, R., Poate, T., van Geer, P., 2014. Modelling storm response on gravel beaches using XBeach-G. Proc. Inst. Civ. Eng. - Marit. Eng. 167, 173–191. https://doi.org/10.1680/maen.14.00020
Masselink, G., Puleo, J.A., 2006. Swash-zone morphodynamics. Cont. Shelf Res. 26, 661–680. https://doi.org/10.1016/j.csr.2006.01.015
Masselink, G., Van Heteren, S., 2014. Response of wave-dominated and mixed-energy barriers to storms. Mar. Geol. 352, 321–347. https://doi.org/10.1016/j.margeo.2013.11.004
Mentaschi, L., Vousdoukas, M.I., Pekel, J.-F., Voukouvalas, E., Feyen, L., 2018. Global long-term observations of coastal erosion and accretion. Sci. Rep. 8, 12876. https://doi.org/10.1038/s41598-018-30904-w
Moore, L.J., 2000. Shoreline mapping techniques. J. Coast. Res. 16, 111–124. https://doi.org/10.2112/03-0071.1
Moore, L.J., Ruggiero, P., List, J.H., 2006. Comparing Mean High Water and High Water Line shorelines: should proxy-datum offsets be incorporated into shoreline change analysis? J. Coast. Res. 22, 894–905. https://doi.org/10.2112/04-0401.1
Moorlock, B.S.P., Booth, S.J., Hamblin, R.J.O., Pawley, S.J., Smith, N.J.P., Woods, M.A., 2008. Geology of the Wells-next-the-Sea district – a brief explanation of the geological map.

Sheet Explanation of the British Geological Survey. 1:50,000 Sheet 130 (England and Wales). Keyworth.
Morton, R.A., Miller, T.L., Moore, L.J., 2004. National assessment of shoreline change: part 1 historical shoreline changes and associated coastal land loss along the U.S. Gulf of Mexico.
Muir Wood, R., Bateman, W., 2005. Uncertainties and constraints on breaching and their implications for flood loss estimation. Philos. Trans. A. Math. Phys. Eng. Sci. 363, 1423–1430. https://doi.org/10.1098/rsta.2005.1576
Neumann, B., Vafeidis, A.T., Zimmermann, J., Nicholls, R.J., 2015. Future coastal population growth and exposure to sea-level rise and coastal flooding - a global assessment. PLoS One 10, 1–34. https://doi.org/10.1371/journal.pone.0118571
Oliver, F.W., 1924. Report of the Blakeney Point research station. For the years 1920 – 1923. Trans. Norfolk Norwich Nat. Soc. 2, 396–422.
Oliver, F.W., 1913. Some remarks on Blakeney Point, Norfolk. J. Ecol. 1, 4–15.
Oliver, R., 1996. Taking to the water: some examples of OS mapping of the coast, in: Sheetlines. The Charles Close Society, pp. 9–27.
Orford, J., Jennings, S., 1998. The importance of different time-scale controls on coastal management strategy: the problem of Porlock gravel barrier, Somerset, UK, in: Hooke, J.M. (Ed.), Coastal Defence and Earth Science Conservation. Geological Society, p. 270.
Orford, J.D., Carter, R.W.G., Jennings, S.C., 1991. Coarse clastic barrier environments: evolution and implications for quaternary sea level interpretation. Quat. Int. 9, 87–104. https://doi.org/10.1016/1040-6182(91)90068-Y
Orford, J.D., Carter, R.W.G., Jennings, S.C., Hinton, A.C., 1995. Processes and timescales by which a coastal gravel-dominated barrier responds geomorphologically to sea-level rise: Story head barrier, Nova Scotia. Earth Surf. Process. Landforms 20, 21–37. https://doi.org/10.1002/esp.3290200104
Orford, J.D., Forbes, D.L., Jennings, S.C., 2002. Organisational controls, typologies and time scales of paraglacial gravel-dominated coastal systems. Geomorphology 48, 51–85. https://doi.org/10.1016/S0169-555X(02)00175-7
Orford, J.D., G Carter, R.W., Jennings, S.C., 1996. Control domains and morphological phases in gravel-dominated coastal barriers of Nova Scotia. J. Coast. Res. 12, 589–604.
Otvos, E.G., 2012. Coastal barriers - nomenclature, processes, and classification issues. Geomorphology 139–140, 39–52. https://doi.org/10.1016/j.geomorph.2011.10.037
Pajak, M.J., Leatherman, S., 2002. The High Water Line as shoreline indicator. J. Coast. Res. 18, 329–337.
Parker, B.B., 2003. The difficulties in measuring a consistently defined shoreline -the problem of vertical referencing. J. Coast. Res. 24, 44–56.
Phillips, J., Van Dyke, C., 2016. Principles of geomorphic disturbance and recovery in response to storms. Earth Surf. Process. Landforms 41, 971–979. https://doi.org/10.1002/esp.3912
Phillips, J.D., 2014. State transitions in geomorphic responses to environmental change.

Geomorphology 204, 208–216. https://doi.org/10.1016/j.geomorph.2013.08.005
Pollard, J.A., Brooks, S.M., Spencer, T., 2019a. Harmonising topographic & remotely sensed datasets, a reference dataset for shoreline and beach change analysis. Nat. Sci. Data 6, 1–14.
Pollard, J.A., Brooks, S.M., Spencer, T., Christie, E.K., Möller, I., 2019b. Will nature work with us? Erosion and flooding impacts on a UK barrier, in: Wang, P., Rosati, J.D., Vallee, M. (Eds.), Coastal Sediments 2019. World Scientific, Tampa, FL, pp. 114–127.
Pollard, J.A., Spencer, T., Jude, S., 2018. Big Data Approaches for coastal flood risk assessment and emergency response. Wiley Interdiscip. Rev. Clim. Chang. 9, e543. https://doi.org/10.1002/wcc.543
Powell, K.A., 1990. Predicting short term profile response for shingle beaches. Hydraulics Research Wallingford.
Robertson, W., Whitman, D., Zhang, K., Leatherman, S.P., 2004. Mapping shoreline position using airborne laser altimetry. J. Coast. Res. 20, 884–892. https://doi.org/10.2112/1551-5036(2004)20[884:MSPUAL]2.0.CO;2
Ruggiero, P., Kaminsky, G.M., Gelfenbaum, G., 2003. Linking proxy-based and datum-based shorelines on a high-energy coastline: implications for shoreline change analyses. J. Coast. Res. Special Is, 57–82.
Rumson, A.G., Hallett, S.H., Brewer, T.R., 2017. Coastal risk adaptation: the potential role of accessible geospatial Big Data. Mar. Policy 83, 100–110. https://doi.org/10.1016/j.marpol.2017.05.032
Schwartz, R.K., 1975. Nature and Genesis of Some Storm Washover Deposits. Springfield, Virginia. https://doi.org/10.13140/RG.2.1.2216.9449
Scott, T., Masselink, G., O'Hare, T., Saulter, A., Poate, T., Russell, P., Davidson, M., Conley, D., 2016. The extreme 2013/2014 winter storms: beach recovery along the southwest coast of England. Mar. Geol. 382, 224–241. https://doi.org/10.1016/j.margeo.2016.10.011
Shennan, I., Bradley, S.L., Edwards, R., 2018. Relative sea-level changes and crustal movements in Britain and Ireland since the Last Glacial Maximum. Quat. Sci. Rev. 188, 143–159. https://doi.org/10.1016/J.QUASCIREV.2018.03.031
Shennan, I., Lambeck, K., Horton, B., Innes, J., Lloyd, J., McArthur, J., Rutherford, M., 2000. Holocene isostasy and relative sea-level changes on the east coast of England. Geol. Soc. London, Spec. Publ. 166, 275–298.
Spencer, T., Brooks, S.M., Evans, B.R., Tempest, J.A., Möller, I., 2015. Southern North Sea storm surge event of 5 December 2013: water levels, waves and coastal impacts. Earth-Science Rev. 146, 120–145. https://doi.org/10.1016/j.earscirev.2015.04.002
Stockdon, H.F., Asbury H., Jr., S., List, J.H., Holman, R.A., 2002. Estimation of shoreline position and change using airborne topographic lidar data. J. Coast. Res. 18, 502–513.
Stutz, M.L., Pilkey, O.H., 2011. Open-ocean barrier islands: global influence of climatic, oceanographic, and depositional settings. J. Coast. Res. 27, 207–222. https://doi.org/10.2112/09-1190.1

Sutherland, J., 2012. Error analysis of Ordnance Survey map tidelines. Proc. Inst. Civ. Eng. - Marit. Eng. 165, 189–197.

Thieler, E.R., Danforth, W.W., 1994. Historical shoreline mapping (I): improving techniques and reducing positioning errors. J. Coast. Res. 10, 549–563.

Van der Wal, D., Wielemaker-Van den Dool, A., Herman, P.M.J., 2008. Spatial patterns, rates and mechanisms of saltmarsh cycles (Westerschelde, The Netherlands). Estuar. Coast. Shelf Sci. 76, 357–368. https://doi.org/10.1016/j.ecss.2007.07.017

Van Wellen, E., Chadwick, A.., Mason, T., 2000. A review and assessment of longshore sediment transport equations for coarse-grained beaches. Coast. Eng. 40, 243–275. https://doi.org/10.1016/S0378-3839(00)00031-4

Viles, H., 2016. Technology and geomorphology: are improvements in data collection techniques transforming geomorphic science? Geomorphology 270, 121–133. https://doi.org/10.1016/j.geomorph.2016.07.011

Vos, K., Harley, M.D., Splinter, K.D., Simmons, J.A., Turner, I.L., 2019. Sub-annual to multi-decadal shoreline variability from publicly available satellite imagery. Coast. Eng. 150, 160–174. https://doi.org/10.1016/J.COASTALENG.2019.04.004

Wolf, J., Flather, R.A., 2005. Modelling waves and surges during the 1953 storm. Philos. Trans. R. Soc. A Math. Phys. Eng. Sci. 363, 1359–1375. https://doi.org/10.1098/rsta.2005.1572